Synthesis of Energy-Bounded Planar Caging Grasps using Persistent Homology

Jeffrey Mahler[1,*], Florian T. Pokorny[1,2,*], Sherdil Niyaz[1], Ken Goldberg[1]

[1]AUTOLAB and Berkeley Artificial Intelligence Research Laboratory
Dept. of IEOR and EECS, University of California, Berkeley, USA
{jmahler, sniyaz, goldberg}@berkeley.edu
[2] CAS/CVAP, KTH Royal Institute of Technology, Sweden
fpokorny@kth.se

Abstract. Caging grasps restrict object motion without requiring complete immobilization, providing a practical alternative to force- and form-closure grasps. In [24], we introduced "energy-bounded caging", an extension that relaxes the requirement of complete caging in the presence of gravity and presented EBCA-2D, an algorithm for analyzing a proposed grasp using α-shapes to lower-bound the escape energy. In this paper, we address the problem of synthesizing energy-bounded cages by identifying optimal gripper and force-direction configurations that require the largest increases in potential energy for the object to escape. We present Energy-Bounded-Cage-Synthesis-2D (EBCS-2D), a sampling-based algorithm that uses persistent homology, a recently-developed multiscale approach for topological analysis, to efficiently compute candidate rigid configurations of obstacles that form energy-bounded cages of an object from an α-shape approximation to the configuration space. EBCS-2D runs in a worst-case $O(s^3 + sn^2)$ time where s is the number of samples, and n is the total number of object and obstacle vertices, where typically $n << s$, and in practice we observe runtimes closer to $O(s)$ for fixed n. We also show that constant velocity pushing in the horizontal plane generates an energy field analogous to gravity in the vertical plane that can be analyzed with our approach. We implement EBCS-2D using the Persistent Homology Algorithms Toolbox (PHAT) and study performance on a set of seven planar objects and four gripper types. Experiments suggest that EBCS-2D takes 2-3 minutes on a 6 core processor with 200,000 pose samples. We also find that an RRT* motion planner is unable to find escape paths with lower energy. Physical experiments suggest that EBCS-2D push grasps are robust to perturbations. Additional proofs, data, and code are available at `http://berkeleyautomation.github.io/caging/`.

1 Introduction

In manufacturing and logistics, there are many applications where parts must be reliably grasped and moved without precise constaints on object pose (as required for example in assembly). Caging configurations, in which an object's mobility is bounded by a set of obstacles such as a gripper and / or an energy

field such as gravity, are a promising alternative to form- and force-closure as they provide robustness to perturbations in object pose.

The standard model of caging (complete caging) considers whether a set of obstacles can be placed in a configuration such that the object cannot escape, meaning that its mobility is restricted to a bounded set in the free configuration space $\mathcal{F}$ [35, 42] as illustrated in the left part of Fig. 1. When an energy-potential $U : \mathcal{C} \times \mathcal{C} \rightarrow \mathbb{R}$ specifying an energy field such as gravity is defined on the configuration space $\mathcal{C}$, the notion of caging can be generalized to *energy-bounded caging* [24], where the object is constrained to a bounded path-component of the subset of the free configuration space $\mathcal{F}$ with energy less than some threshold u. This concept naturally occurs, for example when a constant force-field is acting on the object as illustrated in the middle and left of the figure, where gravity acts in the downward direction and the object can only escape the cage if it is lifted to a configuration with higher energy than the initial configuration $\mathbf{q}_0$. Energy bounded cages also occur in the context of planar pushing.

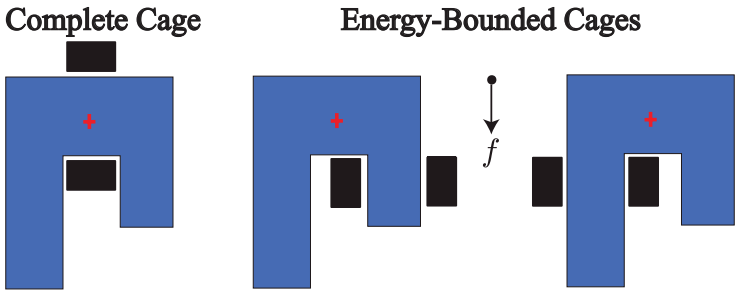

Fig. 1: Complete and energy-bounded cages. Left: a complete cage. The blue object is constrained to a bounded component of the free configuration space by the rigid arrangement of the two gripper fingers (black). Middle and right figure: Two energy-bounded cages with respect to a downward vertical gravity force direction f. The blue object can only escape from its initial configuration when lifted against the gravity field. Note that the rightmost configuration requires more energy to escape.

This paper presents Energy-Bounded-Cage-Synthesis-2D (EBCS-2D), a sampling-based algorithm for synthesis of energy-bounded cages given a polygonal object and a rigid configuration of polygonal obstacles under a convex energy field defined over object translations. EBCS-2D synthesizes an ordered list of energy-bounded cages with minimum escape energy above a threshold using persistent homology, a tool from computational topology that efficiently computes representatives for bounded components of the free configuration over varying escape energy threshold. EBCS-2D constructs a weighted α-shape from samples of object poses and a conservative estimate of their penetration depth [24], finds a set of candidate energy bounded cages using persistence, and prunes the candidates based on collisions and energy level. The escape energies returned by EBCS-2D provably lower bound the true minimum escape energy for each returned cage. If the returned escape energy is infinite then the object is completely caged.

We implement EBCS-2D using the Persistent Homology Algorithms Toolbox (PHAT) [3] to efficiently identify the most robust energy bounded cages. We evaluate EBCS-2D on a set of seven polygonal parts with parallel-jaw grippers using a push energy field and use it to synthesize optimal push directions. In each case, RRT* optimal path planning was unable to find an escape path with lower energy than the estimated lower bound within 120 seconds. We also apply EBCS-2D to the problem of planar pushing on a Zymark Zymate robot and find that configurations synthesized by EBCS-2D successfully push objects on a planar worksurface.

2 Related Work

Complete caging vs energy-bounded caging: The standard concept of caging was introduced by Kuperberg [19] in 1990 and extended by Rimon and Blake [34], which we refer to as "complete" caging. Caging forms an alternative approach to manipulation, distinct from the literature on complete immobilization of an object by means of a form or force closure grasp [29]. Unlike approaches that depend on the local contact geometry, a complete cage of an object causes the object to be constrained to a bounded subset of its free configuration space and requires reasoning about global properties of the configuration space.

Early research on caging studied the caging condition for n points in the plane caging a planar object [19, 35]. Rimon and Blake [34] described the space of cages for a two-finger gripper with one degree of freedom. Sudsang and Ponce [39, 40] proposed caging-based methods for manipulating polygonal objects by means of disc-shaped robots in the plane. Recently, Allen, Burdick and Rimon [2] proposed an algorithm to find all two-finger cage formations of planar polygonal objects by two point-fingers. Vahedi and van der Stappen [42] studied the computation of two and three-finger cages on polygons and used a classification into squeezing and stretching cages. Rodriguez and Mason [37] established and studied caging as a pre-stage to force-closure grasping. Diankov et al. [9] demonstrated that caging grasps can offer beneficial properties for manipulating articulated objects such as door handles.

Recent research has focused on computing cages for specific object families or approximate algorithms due to the difficulty of computing the configuration space for complex gripper and object geometries. These lines of research have primarily focused on synthesizing caging grasps from features in the object surface [33, 20] (e.g. handles) using features of the object surface to rank potential caging hand configurations [25]. Other research has focused on cell-based approximations of the configuration space based on sampling [43]. Mahler et al. [24] defined energy-bounded caging and presented EBCA-2D, an analysis algorithm that can provably lower bound the minimum escape energy to verify energy-bounded cages for a fixed object and obstacle configuration. This paper proposes a synthesis algorithm, Energy-Bounded-Cage-Synthesis-2D (EBCS-2D) and considers energy-bounded cages in the context of planar pushing.

Pushing for manipulation: Constant-velocity quasi-static planar pushing in the horizontal plane can be modelled by an energy potential. Mason introduced

the study of planar pushing to robotics [27] and studied mechanics and planning problems for pushing operations [26]. Peshkin and Sanderson [30] gave a method to find the locus of the centers of rotation of a planar object for all possible pressure distributions of the object on a planar worksurface. Planar pushing can reduce grasp uncertainty using mechanical compliance and can be used to orient parts [1]. Goldberg [17] gave the first complete algorithm for synthesizing a sequence of pushes to orient polygonal parts without sensory feedback. Lynch and Mason investigated controllability of planar pushing, to determine whether an object can be moved between two configurations purely by pushing actions using point and line contacts [23]. Dogar et al. [10] used a physics-based analysis of two-dimensional contact wrenches to compute push-grasps in clutter and proposed a combinatorial search method to plan push-grasps in [11]. Koval et al. [18] decomposed grasping policies into a pre- and post-contact strategy to reduce uncertainty during pushing actions preceding a grasp using a POMDP planner.

Representations and algorithmic approach: We utilize sampling and a discrete representation of the collision space using alpha shapes to reason about cages, building on previous work on motion planning and computational topology. Semi-algebraic functions can be used to prove path non-existence [22], but in practice can be prohibitively expensive to compute. Zhang et al. [45] utilized a rectangular cell-decomposition of the configuration space to prove path non-existence for motion planning by assigning cells to the collision space based on penetration depth. McCarthy et al. [28] use (weighted) α-shapes, a simplicial complex construction defined by Edelsbrunner [13], to represent the collision space from pose samples, and present an algorithm that can prove path non-existence. We build on our previous work [24], which showed that an α-shape-based approximation to the configuration space could be used to analyze a given object and obstacle configuration to check it it is a complete or energy-bounded cage. The present paper also builds on recent advances in topological data analysis [7] and the concept of *persistent homology* [12] to identify "voids" corresponding to cages. Other applications of persistent homology in robotics include methods for clustering trajectories [31] and for motion planning [32, 4].

3 Definitions and Problem Statement

We consider the problem of maximizing the minimum energy required for a rigid polygonal object to escape from a rigid configuration of obstacles on a planar worksurface under a nominal wrench such as pushing or gravity.

Complete Caging and Energy-Bounded Caging

We consider a planar configuration space $\mathcal{C} \subseteq SE(2)$ of a compact polygonal planar object $\mathcal{O} \subset \mathbb{R}^2$ placed in a planar workspace with obstacles defined by fixed positions of a set of k polygons $\mathcal{G} = \mathcal{P}_1 \cup \ldots \cup \mathcal{P}_k \subset \mathbb{R}^2$, such as the jaws of a robotic gripper. We denote the object polygon in pose $\mathbf{q} = (x, y, \theta) \in SE(2) =$

$\mathbb{R}^2 \times \mathbb{S}^1$ relative to a reference pose $\mathbf{q}_0$ by $\mathcal{O}(\mathbf{q})$. We define the *collision space* of $\mathcal{O}$ relative to $\mathcal{G}$ by $\mathcal{Z} = \{\mathbf{q} \in SE(2) : int(\mathcal{O}(\mathbf{q})) \cap \mathcal{G} \neq \emptyset\}$ and denote by $\mathcal{F} = SE(2) - \mathcal{Z}$ the *free configuration space*.

We measure the energy required to move the object between poses by an *energy function* $U : SE(2) \times SE(2) \to \mathbb{R}$ satisfying $U(\mathbf{q}, \mathbf{q}) = 0, \forall \mathbf{q} \in SE(2)$. This is consistent with [24], in which the reference pose was implicit in the energy function. For a fixed threshold $u \in \mathbb{R}$ and reference $\mathbf{q}_0 \in SE(2)$ define the *u-energy forbidden space* by $\mathcal{Z}_u(\mathbf{q}_0) = \mathcal{Z} \cup \{\mathbf{q} \in \mathcal{C} : U(\mathbf{q}, \mathbf{q}_0) > u\}$ and the *u-energy admissible space* $\mathcal{F}_u(\mathbf{q}_0) = SE(2) - \mathcal{Z}_u(\mathbf{q}_0)$. In this work we use the following definitions of caging as in [24] (see Fig. 2):

Definition 1 (Complete and Energy-bounded caging). *A configuration $\mathbf{q}_0 \in \mathcal{F}$ is completely caged if $\mathbf{q}_0$ lies in a compact path-component of $\mathcal{F}$. We call $\mathbf{q}_0$ a* u-energy-bounded cage of $\mathcal{O}$ with respect to U if $\mathbf{q}_0$ lies in a compact path-component of $\mathcal{F}_u(\mathbf{q}_0)$. *Furthermore, the* minimum escape energy, u^*, *for an object $\mathcal{O}$ and obstacle configuration $\mathcal{G}$, is the infimum over values of u such that q is not a u-energy-bounded cage of $\mathcal{O}$, if a finite such u^* exists. Otherwise, we say $u^* = \infty$.*

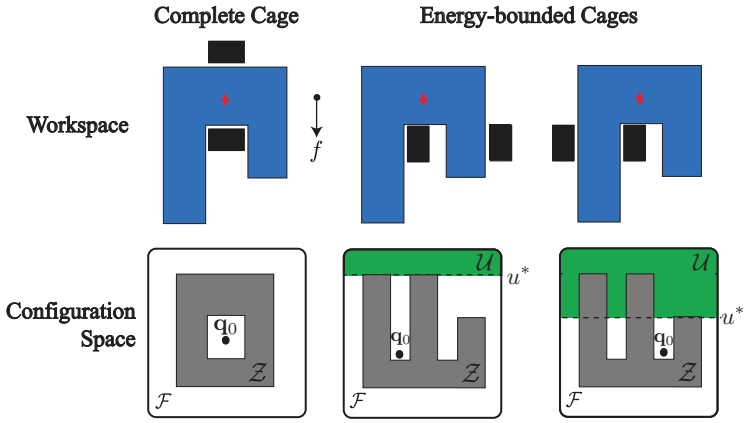

Fig. 2: The top row depicts gripper jaws $\mathcal{G}$ (in black) and an object $\mathcal{O}$ (in blue) in three configurations. The bottom row illustrates conceptually the corresponding point $\mathbf{q}_0 \in SE(2)$ in configuration space. While a complete cage corresponds to an initial pose $\mathbf{q}_0$ completely enclosed by forbidden space $\mathcal{Z}$, the energy-bounded cage on the right instead correpsonds to a case where $\mathbf{q}_0$ is enclosed by $\mathcal{Z}_u = \mathcal{Z} \cup \mathcal{U}(\mathbf{q}_0, u)$ where $\mathcal{U}(\mathbf{q}_0, u) = \{\mathbf{q} \in \mathcal{C} : U(\mathbf{q}, \mathbf{q}_0) > u\}$ for U that is strictly increasing with increasing vertical coordinate. The smallest value of u such that $\mathbf{q}_0$ is not enclosed is called the minimum escape energy, u^*.

While energy-bounded cages can be defined for any energy function U, finding bounded components of $\mathcal{C}$ for all possible pairs of poses in the energy function may be computationally expensive. Thus, for synthesis, we require that the energy function can be derived from a univariate *potential function* $P : SE(2) \to \mathbb{R}$: $U(\mathbf{q}_i, \mathbf{q}_j) = P(\mathbf{q}_i) - P(\mathbf{q}_j)$. In this work, we further assume that P depends only on the translation component $\mathbb{R}^2$ of $SE(2)$ and that P is convex. Given

such an energy field U, our objective is to synthesize all energy-bounded cages $\mathbf{q}_i \in SE(2)$ for an object such that $u_i^* > u_t$ for a given threshold energy u_t.

Energy Functions

We now derive energy functions for gravity in the vertical plane and constant force pushing in the horizontal plane. We develop such functions based on the energy (mechanical work) that wrenches must exert to transport the object between two poses under a nominal wrench resulting from pushing or gravity.

Gravity in the Vertical Plane. Let m denote the mass of the object. Then the energy required to move the object from a reference configuration $\mathbf{q}_i$ to configuration $\mathbf{q}_j$ is $U(\mathbf{q}_j, \mathbf{q}_i) = mg(y_j - y_i)$, where $g = 9.81m/s^2$ is the acceleration due to gravity in the y-direction [16, 24]. This corresponds to the potential $P(\mathbf{q}) = mgy$.

Constant-Velocity Linear Pushing in the Horizonal Plane. Consider an object being pushed along a fixed direction $\hat{\mathbf{v}}$ by a gripper with a constant velocity on a horizonal worksurface under quasi-static conditions and Coloumb friction with uniform coefficient of friction μ [27, 26, 30]. Then energy function $U(\mathbf{q}_j, \mathbf{q}_i) = F_p(\mathcal{O}, \mathcal{G}, \mu)\hat{\mathbf{v}} \cdot (x_j - x_i, y_j - y_i) - \kappa(\mathcal{O}, \mathcal{G}, \mu)$ is a lower bound on the energy required to move the object from pose $\mathbf{q}_i$ to $\mathbf{q}_j$ relative to $\mathcal{G}$, where $F_p(\mathcal{O}, \mathcal{G}, \mu) \in \mathbb{R}$ is a bound on the possible resultant force due to contact between the object and gripper and $\kappa(\mathcal{O}, \mathcal{G}, \mu) \in \mathbb{R}$ is a bound on the possible contact torques and frictional wrenches. A proof is given in the supplemental file at `http://berkeleyautomation.github.io/caging/`. Therefore we propose to use the linear potential $P(\mathbf{q}) = F_p\hat{\mathbf{v}} \cdot (x, y)$ to lower bound the minimum energy required for the object to escape under the nominal push wrench.

Configuration Spaces and α-Complexes

As in [24], we utilize a family of simplicial complexes called α-complexes [13] to approximate the collision space $\mathcal{Z}$ and u-energy forbidden space. For this purpose, we first uniformly sample a collection of s poses $\mathcal{Q} = \{\mathbf{q}_1, \ldots, \mathbf{q}_s\}$, $\mathbf{q}_i = (x_i, y_i, \theta_i)$ in $\mathcal{Z}$ and determine the radius $r(\mathbf{q}_i) > 0$ for each $\mathbf{q}_i$, such that the metric ball $\mathbb{B}(\mathbf{q}_i) = \{\mathbf{q} \in SE(2) : d(\mathbf{q}, \mathbf{q}_i) \leqslant r(\mathbf{q}_i)\}$ is completely contained in $\mathcal{Z}$. These radii are computed using a conservative penetration depth solver and the standard metric d on $SE(2)$; details can be found in [24]. The union of these balls $B(Q) = \cup_{i=1}^{s} \mathbb{B}(\mathbf{q}_i)$ forms a subset of the collision space that provides a conservative approximation of $\mathcal{Z}$. See the left part of Fig. 3 for a conceptual illustration.

Since reasoning about subsets of $\mathbb{R}^3$ instead of $SE(2)$ is advantageous computationally, we follow the approach of [24] to lift the configuration space to $\mathbb{R}^3$. For this purpose, let ρ denote the maximum moment arm of $\mathcal{O}$ and let $\pi : \mathbb{R}^3 \to SE(2)$ be defined by $\pi(x, y, z) = (x, y, (z/\rho) \mod 2\pi)$. We invert this mapping by $\pi_n^{-1}(x, y, \theta) = (x, y, \rho(\theta + 2\pi n))$ for $n \in \mathbb{Z}$ (see [24]). The samples Q are then mapped to $X = \{\hat{\mathbf{q}}_{i,n} = \pi_n^{-1}(\mathbf{q}_i) : \mathbf{q}_i \in Q, n \in \{-R, \ldots, 0, \ldots, R\}\}$ for a chosen integer $R > 1$. We utilize a *simplicial complex* representation of $B(X)$ known as an α-shape [13, 14] to approximate $B(X)$ since its shape is difficult

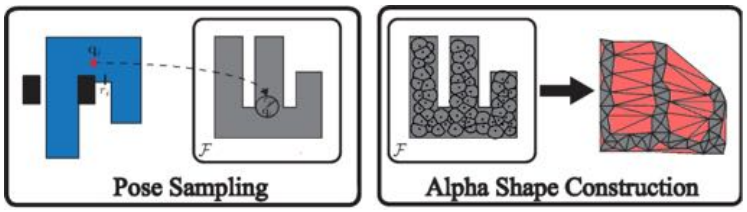

Fig. 3: (Left) An approximation of the forbidden space $\mathcal{Z} \subset SE(2)$ from Fig. 2 by unions of balls around sampled points Q results in (right) an α-shape simplicial complex (gray) that is a subset of the weighted Delaunay triangulation of the sampled points when lifted from $SE(2)$ to $\mathbb{R}^3$. The free space is colored in red.

to analyze computationally. A geometric k-simplex $\sigma = [\mathbf{v}_0, \ldots, \mathbf{v}_k]$ in $\mathbb{R}^d$ is a convex hull of $k+1$ ordered affinely independent elements $\mathbf{v}_0, \ldots, \mathbf{v}_k \in \mathbb{R}^d$ and a convex hull of an ordered subset of these elements is called a face τ of σ, indicated by $\tau \leqslant \sigma$. A finite simplicial complex $\mathcal{K}$ is a non-empty set of simplices such that if $\sigma \in \mathcal{K}$ and $\tau \leqslant \sigma$, then $\tau \in \mathcal{K}$ and if $\sigma, \sigma' \in \mathcal{K}$ then $\sigma \cap \sigma'$ is empty or an element of $\mathcal{K}$. In dimension 3, a simplicial complex $\mathcal{K}$ is a union of points, line-segments, triangles and tetrahedra whose intersections are either empty or another simplex in $\mathcal{K}$, thus generalizing the idea of both a graph and a triangulation in $\mathbb{R}^3$. The α-shape simplicial complex $A(X)$ corresponding to $B(X)$ lies strictly inside $B(X)$ and is homotopy-equivalent to $B(X)$, meaning that topological properties of $B(X)$ can be computed directly from $A(X)$ [13]. Additionally, all simplices in $A(X)$ are contained in the weighted Delaunay triangulation of X which triangulates the convex hull of X and which has to be computed during the construction of $A(X)$. Fig. 3 provides a conceptual illustration where simplices in $A(X)$ are shown in gray and simplices in $D(X) - A(X)$ in red.

Persistent Second Homology

Persistent Homology [12] studies the topological features (e.g. holes, voids) that are created and destroyed over a one parameter family of simplicial complexes called *filtrations*. Fig. Fig. 4 provide a conceptual visualization of 2D slices of "voids" found by persistence for a 3D filtration and a qualitative persistence diagram. A simplex-wise filtration of a simplicial complex $K = \cup_{i=1}^{n} \sigma_i$ is a collection of simplicial complexes K_i such that $K_i = \cup_{i=1}^{i} \sigma_i$, so that K_{i+1} is the result of adding a single simplex σ_{i+1} to K_i. We call i the filtration index. Such a filtration can arise naturally when a function $f : K \to \mathbb{R}$ is defined on the set simplices of K and simplices are ordered in decreasing values of f: $f(\sigma_i) \geqslant f(\sigma_j)$ for all $i \leqslant j$. Thus persistence finds the topological features that emerge as the simplices are added in order of decreasing f. Here, $f(\sigma_i)$ is called the filtration value corresponding to filtration index i. The j-th persistence diagram measures the dimension of the j-th homology group $H_j(K_i)$ that corresponds to a vector space (with finite field coefficients). The dimension of each of these spaces is a topological invariant that does not vary under continuous deformations of

the underlying simplicial complex $H(K_i)$. In this work, we are interested in subcomplexes K_i of the weighted Delaunay triangulation $D(X) \subset \mathbb{R}^3$ and the *second homology group* $H_2(K_i)$. Intuitively, the dimension of the second homology group corresponds to "voids" in K_i which are completely enclosed by the complex K_i. These voids in K_i can appear as we add new simplices with increasing i, or they can disappear as voids are filled in. The second persistence diagram enables us to visualize these topological changes. Each point (x, y) in the diagram corresponds to a pair of filtration indices (i, j) recording the fact that a void has "appeared" at index i and disappeared at index j. For a geometric simplicial complex, these index pairs (i, j) correspond to simplices (σ_i, σ_j) where σ_j is a *tetrahedron* (a 3-simplex) which destroys or "fills in" a void, while σ_i corresponds to a *triangle* (2-simplex) that corresponds to the last complex needed to first create a fully enclosed void. The set of (i, j) pairs can be displayed in the (index)-persistence diagram, or alternatively, when the filtration arises from a function f, we may display the set of points $(f(\sigma_i), f(\sigma_j))$. By considering the vertical distance $f(\sigma_i) - f(\sigma_j)$ from the diagonal, we can read off the parameter range of f during which a void exists in the evolution of the filtration.

4 The EBCS-2D Algorithm

EBCS-2D (Algorithm 1) takes as input a polygonal object $\mathcal{O}$, obstacle configuration $\mathcal{G}$, potential function P, and energy threshold u_t, and outputs a set of energy-bounded cages that require at least u_t energy to escape.

Using uniform sampling, the algorithm first generates s object poses in collision $\mathcal{Q} = \{\mathbf{q}_1, ..., \mathbf{q}_s\}$ and their corresponding penetration depths $\mathcal{R} = \{r_1, ..., r_s\}$. We lift the poses to $\mathbb{R}^3$ and construct an α-shape approximation to the configuration space as described in Section 3. Next, we construct a filtration by sorting all simplices in the free space in order of decreasing energy level and use persistent homology to identify path components fully surrounded by u-energy forbidden space for all u thresholds. Finally, we examine the simplices within each bounded component in order of increasing energy to check for a collision-free object pose, and return the poses extracted from each component. Fig. 4 illustrates the use of persistence in our algorithm.

Filtrations and Persistence from Energy Functions: In order to synthesize energy-bounded cages with persistence, we first order the simplices of the α-shape approximation by decreasing energy level. We assumed that the potential $P : SE(2) \to \mathbb{R}^3$ depends only on the translational component $\mathbb{R}^2$ of $SE(2)$ and is convex on that space. In this case, for any k-simplex $\sigma = \text{Conv}(\mathbf{v}_0, \ldots, \mathbf{v}_k) \in D(X) - A(X)$ we have:

$$\min_{\mathbf{x} \in \sigma} P(\pi(\mathbf{x})) = \min\{P(\pi(\mathbf{v}_0)), \ldots, P(\pi(\mathbf{v}_k))\}.$$

where $\pi : \mathbb{R}^3 \to SE(2)$ denotes the projection to $SE(2)$. Using this fact, we construct a function $D(X) \to \mathbb{R}$:

$$f(\sigma) = \begin{cases} \min_{\mathbf{x} \in \sigma} P(\pi(\mathbf{x})) & \sigma \in D(X) - A(X) \\ \infty & \sigma \in A(X) \end{cases}$$

This gives rise to a filtration $K = K(X, U) : \emptyset = K_0 \subset K_1 \subset \ldots \subset K_n \subset D(X)$ of simplices in $D(X)$ with respect to P as described in Section 3.

EBCS-2D uses persistent homology to find pairs of simplices σ_i, σ_j corresponding to the birth and death, respectively, of a bounded path component $C(X) \subset D(X)$ in the free configuration space. Using the centroid of simplices as candidate energy bounded cages, we then search for the lowest energy collision-free simplex $\sigma \in C(X)$. The algorithm runs in $O(s^3 + sn^2)$ time where s is the number of samples and n is the total number of object and obstacle vertices. This is because α-shape construction is $O(s^2 + sn^2)$ [24, 28] and the boundary matrix reduction used in persistent homology is $O(s^3)$ in the worst case [8].

Input: Polygonal robot gripper $\mathcal{G}$, Polygonal object $\mathcal{O}$, Potential function P, Number of pose samples s, Number of rotations R for $SE(2)$ lifting, Energy threshold u_t
Result: $\hat{\mathcal{Q}}$, set of energy-bounded cages with estimated escape energies
`// Sample poses in collision`
$\mathcal{Q} = \varnothing, R = \varnothing, \ell = diam(\mathcal{G}) + diam(\mathcal{O})$;
$\mathcal{W} = [-\ell, \ell] \times [-\ell, \ell] \times [0, 2\pi)$;
for $i \in \{1, ..., s\}$ **do**
  $\mathbf{q}_i$ = RejectionSample($\mathcal{W}$);
  r_i = LowerBoundPenDepth($\mathbf{q}_i, \mathcal{O}, \mathcal{G}$);
  if $r_i > 0$ **then**
    $\mathcal{Q} = \mathcal{Q} \cup \{\mathbf{q}_i\}$, $R = R \cup \{r_i\}$;
end
$X = \{\pi_n^{-1}(\mathbf{q}_i) \mid \mathbf{q}_i \in \mathcal{Q}, n \in \{-N_r, ..., N_r\}\}$;
`// Create alpha shape`
$D(X, R)$ = WeightedDelaunayTriangulation(X, R);
$A(X, R)$ = WeightedAlphaShape($D(X, R), \alpha = 0$);
`// Run Persistent Homology`
K = Filtration($D(X, R), A(X, R)$);
Δ = ComputeSecondHomologyPersistencePairs(K);
`// Find Energy-Bounded Cages`
for $(i, j) \in \Delta$ **do**
  $C(K_i, \sigma_j)$ = PathComponent(σ_j, K_i);
  for $\sigma \in$ *Sorted(*$C(K_i, \sigma_j)), P$*)* **do**
    $\mathbf{q}$ =Centroid(σ);
    $u = P(\sigma_i) - P(\mathbf{q})$;
    if *CollisionFree(*$\mathbf{q}$*) and* $u > u_t$ **then**
      $\hat{\mathcal{Q}} = \hat{\mathcal{Q}} \cup \{(\mathbf{q}, u)\}$;
    end
  end
end
return $\hat{\mathcal{Q}}$;

Algorithm 1: Energy-Bounded-Cage-Synthesis-2D

Correctness: EBCS-2D returns energy-bounded cages with a provable lower bound on the minimum escape energy:

Theorem 1. *Let* $\hat{\mathcal{Q}} = \{(\hat{\mathbf{q}}_1, \hat{u}_1), ...(\hat{\mathbf{q}}_n, \hat{u}_n)\}$ *denote the energy bounded cages returned by EBCS-2D. For each* $(\hat{\mathbf{q}}_i, \hat{u}_i) \in \hat{\mathcal{Q}}$, $\hat{\mathbf{q}}$ *is a* $\hat{u}$*-energy bounded cage of* $\mathcal{O}$ *with respect to* U*.*

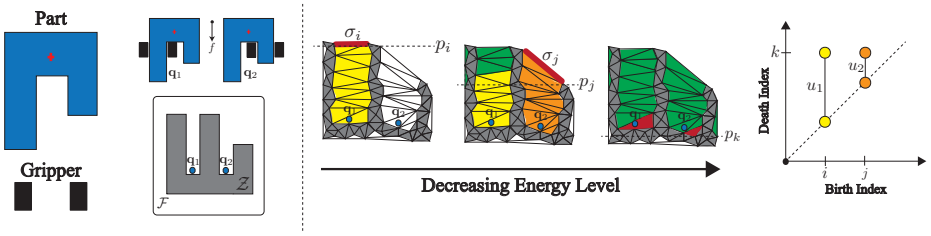

Fig. 4: Persistence diagram for ranking energy-bounded cages. Left: polygonal part and gripper polygons serve as input. We sample object poses X in collision and generate an alpha-shape representation (shown in gray in the three middle figures). Given an energy potential, we insert simplices in $D(X) - A(X)$ in decreasing order of energy potential, creating a filtration of simplicial complexes. Voids (yellow and orange) are born with the addition of edges σ_i and σ_j (red) at threshold potential levels p_i and p_j respectively, and die with the additions of the last triangle in each void at potential p_k (red). The associated second persistence diagram (right figure) reveals voids with large persistence corresponding to energy-bounded cages with energy equal to the difference in potentials: $u_1 = p_k - p_i$ and $u_2 = p_k - p_j$. In particular, configuration $\mathbf{q}_1$ is identified as more persistent (and therefore with higher escape energy) than configuration $\mathbf{q}_2$.

See the supplemental file at `http://berkeleyautomation.github.io/caging/` for a proof.

Extension to Pushing EBCS-2D can be applied to push grasping in the horizontal plane. We use it to find push directions that yield robust energy-bounded cages by running EBCS-2D for a set of sampled push directions using the constant velocity linear push energy of Section 3. The extension runs EBCS-2D using P push angles uniformly sampled from $[\frac{\pi}{2} - \varphi, \frac{\pi}{2} + \varphi]$ and returns a ranked list of push directions and energy-bounded cages that can be reached by a linear, collision-free path along the push direction. While the potential changes for each such push direction, the simplices only need to be re-sorted and therefore the sampling and α-complex construction only need to be performed once.

5 Experiments

We implemented EBCS-2D in C++ and evaluated its performance on a set of polygonal objects under both gravitational and pushing energy fields. We used CGAL [41] to compute α-shapes, the GJK-EPA algorithm of libccd [15] to compute penetration depth, and the twist reduction algorithm implemented in PHAT [3] to compute the second persistence diagram. Our dataset consisted of seven polygonal parts created by triangulating the projections of models from YCB [6] and 3DNet [44] onto a plane. All experiments ran on an Intel Core i7-4770K 350GHz processor with 6 cores.

Energy Bounded Cages Under Linear Push Energy We consider a linear push energy field with a push force bound of $F_p = 1.0$ for the set of parts with

four grippers: rectangular parallel jaws, an overhead projection of a Zymark Zymate gripper with parallel jaws [21], an overhead projection of a Barrett hand with a pregrasping shape inspired by [11], and a four finger disc gripper inspired by [38]. We ran the pushing extension to EBCS-2D for the rectangular parallel jaws, Zymark gripper, and Barrett hand with $s = 200,000$ samples, an energy lower bound of $u_t = 0.5$, an angle limit of $\varphi = \frac{\pi}{4}$, and $P = 5$ push directions to sweep from $-\frac{\pi}{4}$ to $\frac{\pi}{4}$ in intervals of $\frac{\pi}{8}$. For the four finger gripper, we ran EBCS-2D with a fixed vertical push direction to illustrate the ability of our algorithm to prove complete cages EBCS-2D took approximately 170 seconds to run on average for a single push direction. Fig. 5 illustrates configurations synthesized by EBCS-2D with the estimated normalized minimum escape energy $\hat{u}_n = \hat{u}/F_P$, or distance against the linear push energy that the object must travel to escape. To evaluate the lower bound of Theorem 1, we also used RRT* to attempt to plan an object escape path over the set of collision-free poses with energy less than $\hat{u}$, which was not able to find an escape path with energy less than $\hat{u}$ in 120 seconds of planning [24].

Sample and Time Complexity We also studied the sensitivity of the estimated escape energy for the highest energy configurations synthesized by EBCS-2D for a fixed push direction and the algorithm runtime to the number of pose samples s. The left panel of Fig. 6 shows the ratio of $\hat{u}$ for $s \in \{12.5, 25, 50, 100, 200, 400\} \times 10^3$ pose samples to $\hat{u}$ at $s = 400,000$ pose samples for each of the displayed objects and parallel jaw griipers configurations. We averaged the ratios over 5 independent trials per value of s. Object A is only within 80% of the value at $s = 400,000$ after $s = 200,000$ samples, possibly because of the long thin portion of the configuration space as observed in [24]. Objects B and C both converge to within 95% after about $s = 200,000$ samples. This is comparable to the sample complexity for analysis of a single, fixed configuration with EBCA-2D. The right panel of Fig. 6 shows the relationship between the runtime of EBCS-2D in seconds versus the number of pose samples s over 5 independent runs of the algorithm for the same objects. We broke down the run time by the section of the algorithm: sampling poses, constructing the α-shape to aproximate $\mathcal{C}$, sorting the simplices for the filtration, and computing and pruning candidate energy bounded cages with persistence. The runtime is approximately linear in the number of pose samples, and the largest portion of runtime is the time to sample poses and compute penetration depth. This suggests that the runtime is considerably below the worst case s^3 scaling in practice. The persistence diagram computation in particular has been observed to commonly exhibit sub-quadratic runtime [8] despite its worst-case cubic complexity.

Physical Experiments We evaluated the pushes synthesized by EBCS-2D for the three object configurations with the Zymark gripper illustrated in Fig. 5 on a set of extruded fiberboard polygonal parts [21] using a Zymark Zymate robot to push the objects at a constant velocity on a planar worksurface. Fig. 7 illustrates our experiments. For each configuration, the object was placed in the center of a turntable, rotated to align the push direction with the arm's major axis, and

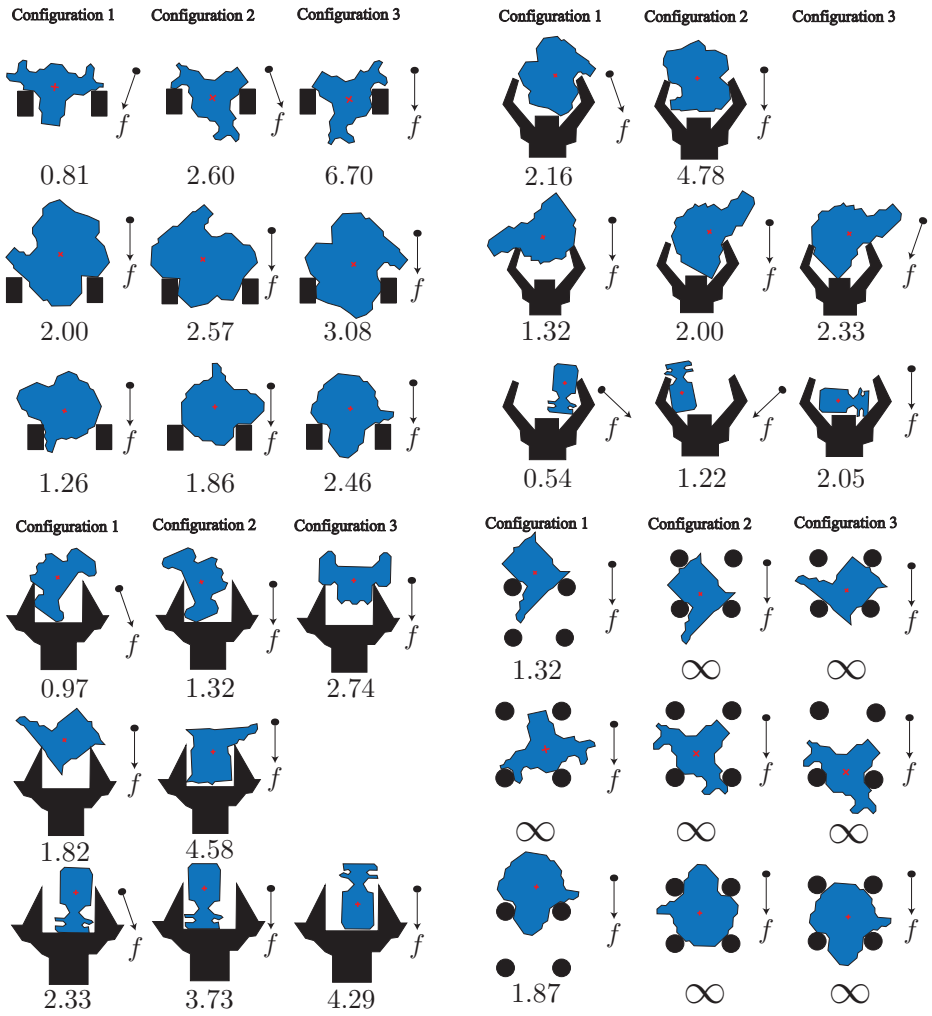

Fig. 5: Illustration of highest energy configurations and push directions synthesized using EBCS-2D ranked from left to right for seven example polygonal objects (blue) and grippers (black) under a linear planar pushing energy field with a push force bound of $F_p = 1.0$. Displayed are three objects for each of the following grippers: (left-to-right, top-to-bottom) parallel-jaw grippers with rectangular jaws, a Barrett hand with fixed preshape, a Zymark Zymate gripper with fixed opening width, and a four finger disc gripper. Below each object is the distance the object would have to travel against the pushing direction, $\hat{u}_n = \hat{u}/F_p$, estimated by EBCS-2D using $s = 200,000$ pose samples, and to the right is the synthesized push energy direction f. For each test case we searched over 5 energy directions from $-\frac{\pi}{4}$ to $\frac{\pi}{4}$ and checked push reachability as described in Section 4 except for the four finger gripper, for which we ran only EBCS-2D to illustrate complete cages. The energy of the synthesized configurations is not always directly related to the depth of the part within the object, such as the first row of results for the parallel jaw and Zymark gripper configurations. EBCA-2D also synthesizes several complete cages for the four finger gripper.

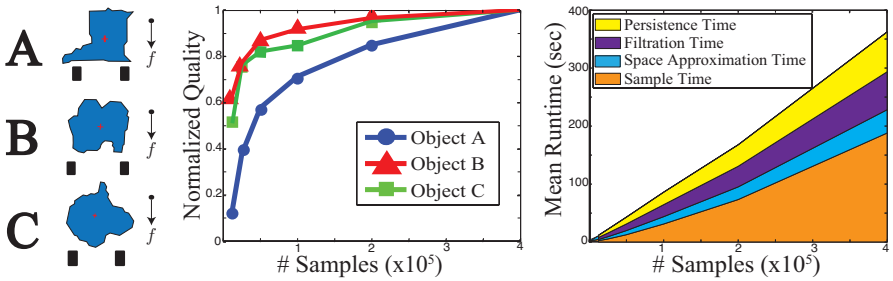

Fig. 6: (Middle) The sample complexity of EBCS-2D. Plotted is the ratio of the highest minimum escape energy out of the energy-bounded cages synthesized by EBCS-2D, $\hat{u}^*$, for the number of pose samples $s = \{12.5, 25, 50, 100, 200, 400\} \times 10^3$ on the object and parallel-jaw displayed on the left. (Right) The mean runtime of EBCS-2D in seconds is broken down by component of the algorithm for varying numbers of pose samples $s = \{12.5, 25, 50, 100, 200, 400\} \times 10^3$. Each datapoint is averaged over five independent runs for each of the object and gripper configurations on the left. Despite the theoretical worst case s^3 runtime, the algorithm runtime is approximately linear in s, and is dominated by sampling time.

pushed forward while the turntable oscillated with an amplitude of ± 0.1 radians to simulate external wrenches on the object. To test robustness we added zero-mean Gaussian noise with standard deviation of 5mm to the gripper translation and 0.04 radians to the gripper rotation in the plane. We then evaluated whether or not the object was captured and remained within the gripper jaws after being pushed 150mm. Pushes planned by EBCS-2D had a success rate of 100% versus 41% for a baseline of pushes planned by choosing gripper poses uniformly at random from (x, y) in the object bounding box and θ in $[0, 2\pi)$.

6 Discussion and Future Work

We present EBCS-2D, an algorithm to synthesize energy-bounded cages for polygonal objects and rigid configurations of objects under a 2D energy field. We also extend EBCS-2D to synthesize push directions under a linear constant velocity push energy field. In future work, we will perform additional experiments and model caging as a pre-stage to force-closure grasping and stretching cages [37, 42]. We also plan to study additional energy-functions to model task-specific caging, and to explore extensions of our algorithms to caging in 3D.

Acknowledgements: This research was performed at the AUTOLAB at UC Berkeley in affiliation with the AMP Lab, BAIR, and the CITRIS "People and Robots" (CPAR) Initiative: http://robotics.citris-uc.org. The authors were supported in part by the U.S. National Science Foundation under NRI Award IIS-1227536: Multilateral Manipulation by Human-Robot Collaborative Systems, the Department of Defense (DoD) through

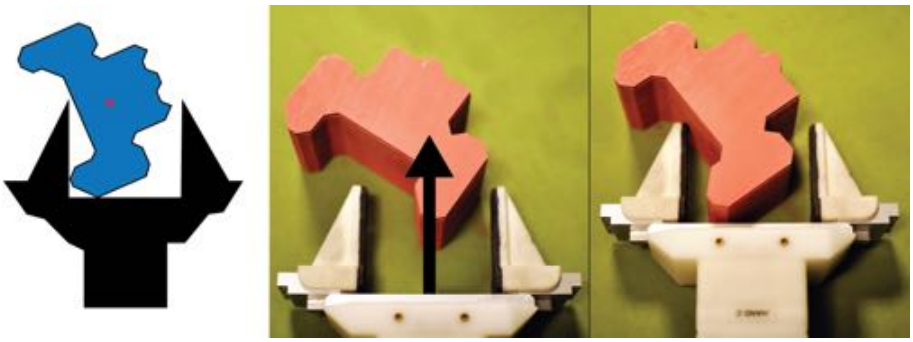

Fig. 7: Illustration of execution of an energy-bounded cage synthesized with EBCS-2D using a Zymark Zymate robot. (Left) The synthesized configuration. (Middle) The planned push direction. (Right) The object remains in the gripper as it is pushed.

the National Defense Science & Engineering Graduate Fellowship (NDSEG) Program, Google, UC Berkeley's Algorithms, Machines, and People Lab, and the Knut and Alice Wallenberg Foundation. We thank our colleagues who provided helpful feedback and suggestions, in particular Subhrajit Bhattacharya, Animesh Garg, David Gealy, Sanjay Krishnan, Michael Laskey, Jacky Liang, Zoe McCarthy, Stephen McKinley, Lauren Miller, and A. Frank van der Stappen.

References

1. S. Akella and M. T. Mason, "Parts orienting by push-aligning," in *Robotics and Automation, 1995. Proceedings., 1995 IEEE International Conference on*, vol. 1. IEEE, 1995, pp. 414–420.
2. T. F. Allen, J. W. Burdick, and E. Rimon, "Two-finger caging of polygonal objects using contact space search," *IEEE Trans. Robotics*, vol. 31, pp. 1164–1179, 2015.
3. U. Bauer, M. Kerber, and J. Reininghaus, "Phat - persistent homology algorithm toolbox," 2013. [Online]. Available: https://code.google.com/p/phat/
4. S. Bhattacharya, R. Ghrist, and V. Kumar, "Persistent homology for path planning in uncertain environments," *IEEE Transactions on Robotics (T-RO)*, March 2015.
5. R. C. Brost, "Automatic grasp planning in the presence of uncertainty," *The International Journal of Robotics Research*, vol. 7, no. 1, pp. 3–17, 1988.
6. B. Calli, A. Walsman, A. Singh, S. Srinivasa, P. Abbeel, and A. M. Dollar, "Benchmarking in manipulation research: The ycb object and model set and benchmarking protocols," *arXiv preprint arXiv:1502.03143*, 2015.
7. G. Carlsson, "Topology and data," *Bull. Amer. Math. Soc. (N.S.)*, vol. 46, no. 2, pp. 255–308, 2009.
8. C. Chen and M. Kerber, "Persistent homology computation with a twist," in *Proceedings 27th European Workshop on Computational Geometry*, vol. 11, 2011.
9. R. Diankov, S. S. Srinivasa, D. Ferguson, and J. Kuffner, "Manipulation planning with caging grasps," in *Humanoid Robots, 2008. Humanoids 2008. 8th IEEE-RAS International Conference on.* IEEE, 2008, pp. 285–292.

10. M. Dogar, K. Hsiao, M. Ciocarlie, and S. Srinivasa, "Physics-based grasp planning through clutter," in *Robotics: Science and Systems VIII*, 2012.
11. M. Dogar and S. Srinivasa, "A framework for push-grasping in clutter," *Robotics: Science and systems VII*, vol. 1, 2011.
12. H. Edelsbrunner and J. Harer, "Persistent homology-a survey," *Contemporary mathematics*, vol. 453, pp. 257–282, 2008.
13. H. Edelsbrunner, *Weighted alpha shapes*. University of Illinois at Urbana-Champaign, Department of Computer Science, 1992.
14. H. Edelsbrunner and J. Harer, *Computational topology: an introduction*. American Mathematical Soc., 2010.
15. D. Fiser, "libccd - collision detection between convex shapes," http://libccd.danfis.cz/.
16. D. C. Giancoli, *Physics: principles with applications*. Pearson Education, 2005.
17. K. Y. Goldberg, "Orienting polygonal parts without sensors," *Algorithmica*, vol. 10, no. 2-4, pp. 201–225, 1993.
18. M. C. Koval, N. S. Pollard, and S. S. Srinivasa, "Pre-and post-contact policy decomposition for planar contact manipulation under uncertainty," *The International Journal of Robotics Research*, vol. 35, no. 1-3, pp. 244–264, 2016.
19. W. Kuperberg, "Problems on polytopes and convex sets," in *DIMACS Workshop on polytopes*, 1990, pp. 584–589.
20. T. H. Kwok, W. Wan, J. Pan, C. C. Wang, J. Yuan, K. Harada, and Y. Chen, "Rope caging and grasping," in *Proc. IEEE Int. Conf. Robotics and Automation (ICRA)*, 2016.
21. M. Laskey, J. Lee, C. Chuck, D. Gealy, W. Hsieh, F. T. Pokorny, A. D. Dragan, and K. Goldberg, "Robot grasping in clutter: Using a hierarchy of supervisors for learning from demonstrations," in *Proc. IEEE Conf. on Automation Science and Engineering (CASE)*. IEEE, 2016.
22. S. M. LaValle, *Planning algorithms*. Cambridge university press, 2006.
23. K. M. Lynch and M. T. Mason, "Controllability of pushing," in *Robotics and Automation, 1995. Proceedings., 1995 IEEE International Conference on*, vol. 1. IEEE, 1995, pp. 112–119.
24. J. Mahler, F. T. Pokorny, A. F. van der Stappen, and K. Goldberg, "Energy-bounded caging: Formal definition and 2d lower bound algorithm based on weighted alpha shapes," in *IEEE Robotics & Automation Letters*. IEEE, 2016.
25. T. Makapunyo, T. Phoka, P. Pipattanasomporn, N. Niparnan, and A. Sudsang, "Measurement framework of partial cage quality based on probabilistic motion planning," in *IEEE Int. Conf. on Robotics and Automation (ICRA)*, 2013, pp. 1574–1579.
26. M. T. Mason, "Mechanics and planning of manipulator pushing operations," *The International Journal of Robotics Research*, vol. 5, no. 3, pp. 53–71, 1986.
27. ——, *Mechanics of Robotic Manipulation*. Cambridge, MA, USA: MIT Press, 2001.
28. Z. McCarthy, T. Bretl, and S. Hutchinson, "Proving path non-existence using sampling and alpha shapes," in *Robotics and Automation (ICRA), 2012 IEEE International Conference on*. IEEE, 2012, pp. 2563–2569.
29. R. M. Murray, Z. Li, and S. S. Sastry, *A mathematical introduction to robotic manipulation*. CRC press, 1994.
30. M. A. Peshkin and A. C. Sanderson, "The motion of a pushed, sliding workpiece," *IEEE Journal on Robotics and Automation*, vol. 4, no. 6, pp. 569–598, 1988.

31. F. T. Pokorny, M. Hawasly, and S. Ramamoorthy, "Multiscale topological trajectory classification with persistent homology," in *Proceedings of Robotics: Science and Systems*, July 2014.
32. F. T. Pokorny and D. Kragic, "Data-driven topological motion planning with persistent cohomology," in *Proceedings of Robotics: Science and Systems*, Rome, Italy, July 2015.
33. F. T. Pokorny, J. A. Stork, and D. Kragic, "Grasping objects with holes: A topological approach," in *Proc. of the IEEE International Conference on Robotics and Automation (ICRA)*, Karlsruhe, Germany, 2013.
34. E. Rimon and A. Blake, "Caging 2d bodies by 1-parameter two-fingered gripping systems," in *Proc. IEEE Int. Conf. Robotics and Automation (ICRA)*, 1996, pp. 1458–1464.
35. E. Rimon and J. W. Burdick, "Mobility of bodies in contact. i. A 2nd-order mobility index for multiple-finger grasps," vol. 14, no. 5, 1998, pp. 696–708.
36. A. Rodriguez and M. T. Mason, "Two finger caging: squeezing and stretching," in *Algorithmic foundation of robotics viii*. Springer Berlin Heidelberg, 2009, pp. 119–133.
37. A. Rodriguez, M. T. Mason, and S. Ferry, "From caging to grasping," *Int. J. Robotics Research (IJRR)*, pp. 1–15, 2012.
38. J. Su, H. Qiao, Z. Ou, and Z.-Y. Liu, "Vision-based caging grasps of polyhedron-like workpieces with a binary industrial gripper," *IEEE Transactions on Automation Science and Engineering*, vol. 12, no. 3, pp. 1033–1046, 2015.
39. A. Sudsang and J. Ponce, "On grasping and manipulating polygonal objects with disc-shaped robots in the plane," in *Proc. IEEE Int. Conf. Robotics and Automation (ICRA)*, 1998, pp. 2740–2746.
40. ——, "A new approach to motion planning for disc-shaped robots manipulating a polygonal object in the plane," in *Robotics and Automation, 2000. Proceedings. ICRA'00. IEEE International Conference on*, vol. 2. IEEE, 2000, pp. 1068–1075.
41. The CGAL Project, *CGAL User and Reference Manual*, 4th ed. CGAL Editorial Board, 2015.
42. M. Vahedi and A. F. van der Stappen, "Caging polygons with two and three fingers," *The International Journal of Robotics Research*, vol. 27, no. 11-12, pp. 1308–1324, 2008.
43. W. Wan, R. Fukui, M. Shimosaka, T. Sato, and Y. Kuniyoshi, "A new grasping by caging solution by using eigen-shapes and space mapping," in *Proc. IEEE Int. Conf. Robotics and Automation (ICRA)*. IEEE, 2013, pp. 1566–1573.
44. W. Wohlkinger, A. Aldoma, R. B. Rusu, and M. Vincze, "3dnet: Large-scale object class recognition from cad models," in *Proc. IEEE Int. Conf. Robotics and Automation (ICRA)*, 2012, pp. 5384–5391.
45. L. Zhang, Y. J. Kim, and D. Manocha, "Efficient cell labelling and path nonexistence computation using c-obstacle query," *The International Journal of Robotics Research*, vol. 27, no. 11-12, pp. 1246–1257, 2008.
46. L. Zhang, Y. J. Kim, G. Varadhan, and D. Manocha, "Fast c-obstacle query computation for motion planning," in *Robotics and Automation, 2006. ICRA 2006. Proceedings 2006 IEEE International Conference on*. IEEE, 2006, pp. 3035–3040.